



Contents lists available at ScienceDirect

Chemical Physics

journal homepage: [www.elsevier.com/locate/chemphys](http://www.elsevier.com/locate/chemphys)

# Ultrafast nonradiative transition pathways in photo-excited pyrazine: *Ab initio* analysis of time-resolved vacuum ultraviolet photoelectron spectrum

Benoît Mignolet<sup>a</sup>, Manabu Kanno<sup>b,\*</sup>, Noriyuki Shimakura<sup>c</sup>, Shiro Koseki<sup>d</sup>, Françoise Remacle<sup>a</sup>, Hirohiko Kono<sup>b</sup>, Yuichi Fujimura<sup>b,e</sup>

<sup>a</sup> Theoretical Physical Chemistry, UR MOLSYS, University of Liège, B4000 Liège, Belgium

<sup>b</sup> Department of Chemistry, Graduate School of Science, Tohoku University, Sendai 980-8578, Japan

<sup>c</sup> Department of Chemistry, Niigata University, Ikarashi Nino-cho 8050, Niigata 950-2181, Japan

<sup>d</sup> Department of Chemistry, Graduate School of Science, and Research Institute for Molecular Electronic Devices (RIMED), Osaka Prefecture University, 1-1 Gakuen-cho, Naka-ku, Sakai 599-8531, Japan

<sup>e</sup> Department of Applied Chemistry, Institute of Molecular Science, and Center for Interdisciplinary Molecular Science, National Chiao-Tung University, Hsin-Chu 300, Taiwan

## ARTICLE INFO

### Keywords:

Pyrazine

Internal conversion

Dark states

Vacuum ultraviolet laser

Photoelectron spectrum

## ABSTRACT

The internal conversion of photo-excited pyrazine, which occurs rapidly on a time scale of about 20 fs, has long been considered to proceed via a conical intersection between the optically bright  $S_2$  ( ${}^1B_{2u}, \pi\pi^*$ ) and dark  $S_1$  ( ${}^1B_{3u}, n\pi^*$ ) states. Since 2008, several theoretical studies have raised the possibility that other dark states  $S_3$  ( ${}^1A_u, n\pi^*$ ) and  $S_4$  ( ${}^1B_{2g}, n\pi^*$ ) may participate dominantly in the early stage of the nonradiative decay of  $S_2$ . To clarify this issue, being motivated by the recent pump-probe experiment by Horio et al. [J. Chem. Phys. 145 (2016) 044306], we calculated vacuum ultraviolet photoelectron spectra for ionization from each of the four excited states. Comparison was made with the measured time-resolved photoelectron spectrum exhibiting a temporally varying multi-band structure. We confirmed no contribution of  $S_3$  or  $S_4$  and thus the validity of the conventional two-state ( $S_2 \rightarrow S_1$ ) picture for ultrafast nonradiative transition in pyrazine.

## 1. Introduction

Pyrazine is a typical azabenzene that undergoes ultrafast nonradiative transitions after ultraviolet (UV) excitation [1–3]. Diffuse bands in UV absorption spectrum of vapor pyrazine are an evidence of the ultrafast nonradiative transition [4]. Femtosecond time-resolved photoelectron measurements provided the transition rate constant of about 20 fs [5,6]. There have been a lot of publications on the mechanism of the ultrafast nonradiative transition in pyrazine since 1980s. Even now there are hot discussions about its origin. Elucidation of the interactions between two types of electronic excited states,  $\pi\pi^*$  and  $n\pi^*$  states, is the key to account for the ultrafast nonradiative transition. Domcke and coworkers theoretically characterized its mechanism within a two-excited-state model, in which the optically bright  $S_2$  ( ${}^1B_{2u}, \pi\pi^*$ ) and dark  $S_1$  ( ${}^1B_{3u}, n\pi^*$ ) states are taken into account [7–15]. They explained that the ultrafast nonradiative transition is due to internal conversion from  $S_2$  to  $S_1$  through a conical intersection.

In the last ten years, a fundamental question has been raised whether other pathways participate in the ultrafast nonradiative transition

of pyrazine [16–19]. In fact, a couple of dark  $n\pi^*$  states were theoretically predicted to locate near  $S_1$  [20] and spectroscopically identified [21,22]. Werner et al. proposed other nonradiative transition pathways via optically dark states,  $S_3$  ( ${}^1A_u, n\pi^*$ ) and  $S_4$  ( ${}^1B_{2g}, n\pi^*$ ), as well as the direct one from  $S_2$  to  $S_1$  [16]. Here, we designate  $S_1$  to  $S_4$  in the order of their electronic energies measured at the Franck-Condon position [21]. Werner et al. calculated time-dependent populations of the four excited states by using the “on-the-fly” time-dependent density functional theory (TDDFT). Here, nonadiabatic transitions were treated with the semiclassical fewest-switches surface hopping procedure [23]. Surprisingly,  $S_3$  and  $S_4$  acquired almost 60% of the initial  $S_2$  population in total at the early stage of nonradiative transition ( $\sim 10$  fs). Sala et al. have also pursued the investigation of the role of the dark  $n\pi^*$  states [18]. They performed the multiconfiguration time-dependent Hartree calculations with the four excited states in a 16-mode model Hamiltonian constructed by using the extended multiconfiguration quasi-degenerate second-order perturbation theory (XMCQDPT2). Their results showed a noticeable participation of  $S_3$  but not of  $S_4$  in the nonradiative transition pathways. It should be noted that, first, the electronic state

\* Corresponding author.

E-mail address: [kanno@m.tohoku.ac.jp](mailto:kanno@m.tohoku.ac.jp) (M. Kanno).

<https://doi.org/10.1016/j.chemphys.2018.07.015>

calculations in the TDDFT and XMCQDPT2 treatments provided low vertical excitation energy to  $S_3$ . Second, in general, the nonadiabatic coupling term has no phase information in the semiclassical surface hopping procedure.

To examine the participation of dark  $n\pi^*$  states by properly taking into account quantum effects in the nonradiative transitions, we performed nuclear wave packet simulations [24]. The potential energy surfaces of  $S_1$  through  $S_4$  were calculated using the multireference configuration interaction (MRCI) method, and their couplings were evaluated within two-dimensional sub-spaces spanned by selected ground-state normal coordinates. Contrary to the results obtained by Werner et al. [16] and Sala et al. [18], our nuclear wave packet simulations demonstrated that nonadiabatic transitions to  $S_3$  and  $S_4$  are so small that the conventional two-state ( $S_2 \rightarrow S_1$ ) picture proposed by Domcke et al. [7–15] is valid.

Soon after our publication [24], Sala et al. proposed a new mechanism for the nonradiative decay processes involving a conical intersection between  $S_3$  and the ground state  $S_0$  ( $^1A_g$ ) [19]. That is, after excitation to  $S_2$ , pyrazine decays to both  $S_1$  and  $S_3$  on an ultrashort time scale of approximately 20 fs. Then, nonradiative transition takes place from  $S_3$  to  $S_0$  on a longer time scale. It still remains ambiguous whether the dark  $n\pi^*$  states other than  $S_1$  make a significant contribution to the nonradiative transitions or not.

Recently, Horio et al. have demonstrated a full observation of the nonradiative decay of  $S_2$  by time-resolved photoelectron spectroscopy with intense 9.3-eV vacuum UV (VUV) probe pulses [25]. Photoelectron spectroscopy is a powerful tool for detecting dark states as well as bright states since any molecular state can be ionized [26]. Compared to their previous experiments with 6.3-eV UV probe pulses that detected ionizations to the lowest two cationic doublet states  $D_0$  ( $^2A_g$ ) and  $D_1$  ( $^2B_{1g}$ ) [6,27], such a VUV photon enabled the access to higher doublet states as well. The measured time-resolved photoelectron spectrum exhibited a characteristic multi-band structure that varied rapidly and dramatically as a function of the pump–probe delay time owing to ultrafast nonradiative transitions. Detailed analysis of the time evolution of this spectrum is expected to offer a convincing answer to the unsolved question of nonradiative transition pathways; however, most previous reports on the simulation of time-resolved photoelectron spectra of pyrazine [12,16,17,28–32] dealt with two ionization channels  $D_1 \leftarrow S_2$  and  $D_0 \leftarrow S_1$  only, which energetically overlap with each other and thus form a single spectral band.

In this paper, a theoretical analysis of the time-resolved VUV photoelectron spectroscopic experiment by Horio et al. [25] is presented including  $S_3$  and  $S_4$  as well as higher cationic doublet states than  $D_1$ . We calculate neutral and cationic electronic states of pyrazine using the MRCI method. The photoelectron spectra are then computed for ionization from each of the four singlet excited states  $S_1$ ,  $S_2$ ,  $S_3$ , and  $S_4$  under the sudden ionization approximation [33,34], which is valid for UV-pump VUV-probe ionizations. Molecular deformation is considered along the totally symmetric  $a_g$  vibrational mode often denoted  $Q_{6a}$  to which a vibrational quantum beat observed in temporal profiles of photoelectron signals of pyrazine was attributed [6].

In the next section, we outline our electronic structure computations based on the MRCI method and the expression for photoelectron spectra within the sudden ionization approximation [33,34]. In Section 3, the calculated photoelectron spectra are compared to the respective experimental ones. We identify the ionization channels that constitute each spectral band appearing in the measurement by Horio et al. [25] and finally confirm that our previous conclusion in Ref. [24] is unchanged, that is, internal conversion proceeds directly from  $S_2$  to  $S_1$  in photo-excited pyrazine. In Section 4, we conclude with an outlook on our future research.

## 2. Computational method

### 2.1. Electronic structure computations for neutral and cationic pyrazine

For neutral pyrazine, we adopt our previous electronic structure results reported in Ref. [24]. The computational outline is given below in brief. The optimized geometry and harmonic vibrational normal modes in the ground state  $S_0$  ( $^1A_g$ ) of  $D_{2h}$  neutral pyrazine were obtained at the complete-active-space self-consistent field (CASSCF) [35,36] level of theory, which allows for static electron correlation, with an active space consisting of ten electrons and eight orbitals (three  $\pi$ , three  $\pi^*$ , and two non-bonding lone-pair orbitals). The CASSCF orbitals were averaged over the states of interest ( $S_0$ – $S_4$ ) with equal weights. These states were then refined by adding dynamic electron correlation using the internally contracted MRCI including single and double excitations to the external space (MRCISD) [37–39]. To lessen computational demands, the six atomic inner-shell orbitals were doubly occupied in all configurations and uncorrelated as frozen-core orbitals. These calculations were executed with the 6–311 +  $G^{**}$  Gaussian basis set [40] by using the *ab initio* quantum chemistry software package MOLPRO [41,42]. The CASSCF/MRCISD treatment overestimated the measured excitation energies from  $S_0$  to  $S_1$ ,  $S_2$ ,  $S_3$ , and  $S_4$  but reproduced the relative energies among the four singlet excited states much better than perturbative methods such as TDDFT and XMCQDPT2, which gave inconsistent results with spectroscopic ones [24].

The doublet electronic states of a singly charged pyrazine cation were computed in the same manner except that the number of active electrons was decreased by one. The reliability of the CASSCF/MRCISD treatment for cationic doublet states will be discussed in Section 3.1.

### 2.2. Computation of photoelectron spectra

A central quantity in the computation of photoelectron spectra is the photoionization matrix element [43] expressed as the dipolar coupling between the wave function of a neutral electronic excited state,  $\Psi_I^{neut}(\mathbf{R})$ , and that of an ionized state, where  $\mathbf{R}$  is a nuclear position. We focus here on the variation of photoelectron spectra as a function of  $\mathbf{R}$  along the totally symmetric mode  $Q_{6a}$ . The coupling elements are given by

$$D_{IK\varepsilon\Omega}(\mathbf{R}) = \langle \Psi_I^{neut}(\mathbf{R}) | \boldsymbol{\mu} | \Psi_K^{cat}(\mathbf{R}), \Psi_{\varepsilon\Omega}^{elec} \rangle, \quad (1)$$

where  $\boldsymbol{\mu}$  is the electric dipole moment operator and the ionized state is defined as the antisymmetrized product of the wave function of a cationic state,  $\Psi_K^{cat}(\mathbf{R})$ , and that of the ionized electron,  $\Psi_{\varepsilon\Omega}^{elec}$ , chosen to be a plane wave. Here,  $\varepsilon$  and  $\Omega$  denote the kinetic energy and emission angle of the photoelectron, respectively. The  $n$ -electron integral is written in the Dirac bra-ket notation, where  $n$  is the number of electrons in the neutral.

The photoionization matrix elements in Eq. (1) can be rewritten as a one-electron integral with the electronic coordinate  $\mathbf{r}$  in the form

$$D_{IK\varepsilon\Omega}(\mathbf{R}) = \langle \phi_{IK}^{Dyson}(\mathbf{R}; \mathbf{r}) | \boldsymbol{\mu} | \Psi_{\varepsilon\Omega}^{elec}(\mathbf{r}) \rangle, \quad (2)$$

where  $\phi_{IK}^{Dyson}(\mathbf{R}; \mathbf{r})$  is the Dyson orbital [44–46], i.e., the overlap between the neutral and cationic electronic states. Its explicit expression is

$$\phi_{IK}^{Dyson}(\mathbf{R}; \mathbf{r}) = \sqrt{n} \int \Psi_I^{neut}(\mathbf{R}; \mathbf{r}, \mathbf{r}_2, \dots, \mathbf{r}_n) \Psi_K^{cat}(\mathbf{R}; \mathbf{r}_2, \dots, \mathbf{r}_n) d\mathbf{r}_2 \dots d\mathbf{r}_n \quad (3)$$

We computed the Dyson orbitals from the MRCISD wave functions of the neutral and cationic states of pyrazine.

The photoelectron spectrum from a neutral state  $I$  at a nuclear position  $\mathbf{R}$  can be computed from the photoionization coupling elements: [2,47]

$$\sigma_I(\mathbf{R}, \varepsilon) \propto \sum_K \delta(\hbar\omega - IP_{IK}(\mathbf{R}) - \varepsilon) \int |D_{IK\varepsilon\Omega}(\mathbf{R})|^2 d\Omega, \quad (4)$$

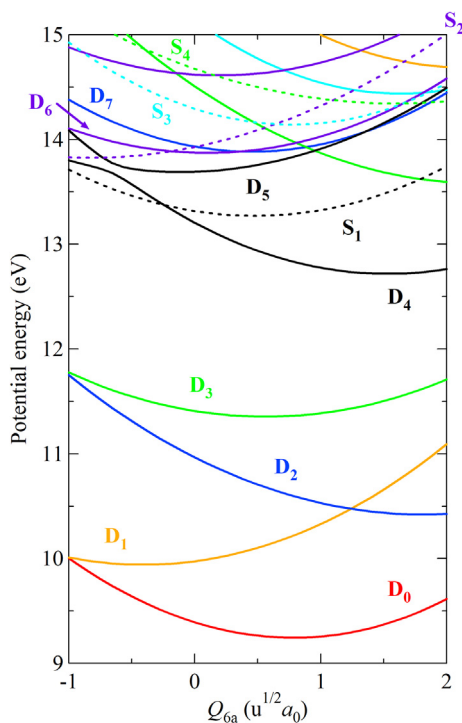


**Fig. 1.** Potential energy curves along the  $Q_{6a}$  mode relative to the energy of  $S_0$  ( $^1A_g$ ) at its optimized geometry. The solid and dotted lines denote those of cationic doublet states [ $D_0$  ( $^2A_g$ ),  $D_1$  ( $^2B_{1g}$ ), etc.] and neutral singlet excited states [ $S_1$  ( $^1B_{3u}$ ),  $S_2$  ( $^1B_{2u}$ ),  $S_3$  ( $^1A_u$ ), and  $S_4$  ( $^1B_{2g}$ )], respectively. The latter are lowered by 0.53 eV to be closer to the experimental data in Table 1 and then dressed by a 9.3-eV photon. The line color indicates the irreducible representation of each state (red, orange, green, light blue, deep blue, purple, and black for  $A_g$ ,  $B_{1g}$ ,  $B_{2g}$ ,  $A_u$ ,  $B_{1u}$ ,  $B_{2u}$ , and  $B_{3u}$ , respectively). (For interpretation of the references to colour in this figure legend, the reader is referred to the web version of this article.)

where  $\hbar\omega$  is the photon energy,  $IP_{IK}(\mathbf{R})$  is the vertical ionization energy between the neutral and cationic states, and  $\delta$  is the Dirac delta function. The photoelectron spectrum in Eq. (4) is composed of a set of discrete peaks. In the results reported below, each peak is a Lorentzian function [48,49] (with a width of 0.5 eV) to account for homogeneous broadening.

### 3. Results and discussion

#### 3.1. Potential energy curves along the $Q_{6a}$ mode

The  $Q_{6a}$  mode induces a totally symmetric in-plane ring deformation, which maintains the  $D_{2h}$  point group symmetry of pyrazine, and hence the irreducible representations of its electronic states are unchanged by a nuclear displacement in this direction. The solid lines in Fig. 1 denote the potential energy curves of cationic doublet states along the  $Q_{6a}$  normal mode in  $S_0$ . Here, the energy of  $S_0$  at its optimized geometry (Franck-Condon position) is set to zero. Similarly to singlet states, we refer to the doublet states as  $D_0$ ,  $D_1$ , etc. in the increasing order of energy at the Franck-Condon position regardless of the value of  $Q_{6a}$ , though many potential crossings are seen in Fig. 1. The potential minimum of  $D_0$  ( $^2A_g$ ) is found at  $Q_{6a} = 0.79 u^{1/2}a_0$  and that of  $D_1$  ( $^2B_{1g}$ ) is located at  $Q_{6a} = -0.41 u^{1/2}a_0$ , where  $u$  is the unified atomic mass unit and  $a_0$  is the Bohr radius. They are fairly close to the respective experimental adiabatic ionization energies from  $S_0$  listed in Table 1; in particular, the deviation for  $D_0$  is merely 0.04 eV. In contrast, the potential minima of  $S_1$  and  $S_2$  reported in Ref. [24] are higher than the corresponding measured adiabatic excitation energies from  $S_0$  in Table 1 by 0.67 and 0.37 eV, respectively. To remedy this problem, we

**Table 1**

Experimental adiabatic excitation/ionization energies from the neutral ground state  $S_0$  ( $^1A_g$ ) and calculated potential minima along  $Q_{6a}$  in units of eV.

State	Exp.	MRCISD
$D_1$ ( $^2B_{1g}$ )	10.169 <sup>a</sup>	9.94
$D_0$ ( $^2A_g$ )	9.288 <sup>a</sup>	9.24
$S_2$ ( $^1B_{2u}$ )	4.69 <sup>b</sup>	5.06 <sup>d</sup>
$S_1$ ( $^1B_{3u}$ )	3.83 <sup>c</sup>	4.50 <sup>d</sup>

<sup>a</sup> Ref. [50].

<sup>b</sup> Ref. [51].

<sup>c</sup> Ref. [1].

<sup>d</sup> Ref. [24].

lowered the MRCISD energies of all the four singlet excited states by 0.53 eV (average of 0.67 and 0.37 eV) in the subsequent calculations of photoelectron spectra. The dotted lines in Fig. 1 represent their corrected potential energy curves along  $Q_{6a}$ , which are additionally shifted by 9.3 eV (photon energy of VUV probe pulses used in the experiment by Horio et al. [25]). For each of the singlet states, only the doublet states below its laser-dressed potential energy curves may be reached with the photon; for example, at the Franck-Condon position  $Q_{6a} = 0$ ,  $D_0$  to  $D_6$  ( $^2B_{2u}$ ) are energetically accessible from  $S_2$ .

#### 3.2. Comparison between experimental and calculated photoelectron spectra

The time-resolved photoelectron spectrum of pyrazine measured in the UV-pump VUV-probe experiment by Horio et al. has shown a drastic change in its band structure as the pump-probe delay time increases [25]. Fig. 2(a) displays their experimental spectra observed at delay times 1 and 49 fs. The former exhibits three bands at a photoelectron kinetic energy of 0–1, 1.5–2.5, and 3.2–4.2 eV. The second band at 1.5–2.5 eV disappears in the latter, while the other two bands are greatly enhanced. The first (near-threshold) band at 0–1 eV and the third one at 3.2–4.2 eV slightly shift to higher and lower kinetic energies, respectively. The first band is strongest regardless of the delay time.

For comparison with the experimental spectra in Fig. 2(a), photoelectron spectra for ionization from each of the four singlet excited states were computed from Eq. (4). We evaluated the spectrum from  $S_2$

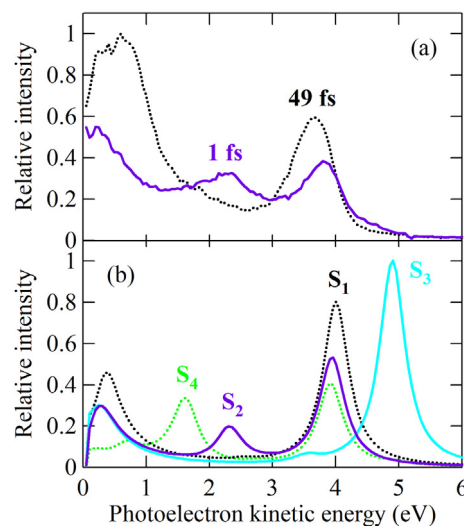


**Fig. 2.** (a) Experimental photoelectron spectra for pump-probe delay times 1 and 49 fs reported in Ref. [25]. (b) Calculated photoelectron spectrum from  $S_2$  ( $^1B_{2u}$ ) at the Franck-Condon position  $Q_{6a} = 0$  and those from  $S_1$  ( $^1B_{3u}$ ),  $S_3$  ( $^1A_u$ ), and  $S_4$  ( $^1B_{2g}$ ) at their potential minima  $Q_{6a} = 0.48, 0.77, \text{ and } 1.59 u^{1/2}a_0$ , respectively.

**Table 2**

Summary of the eleven ionization channels contributing to the calculated photoelectron spectra in Fig. 2(b). The difference between the potential energy curves of laser-dressed singlet states and doublet states in Fig. 1 is denoted as  $\epsilon_c$ . The values of  $Q_{6a}$  and  $\epsilon_c$  are given in units of  $u^{1/2}a_0$  and eV, respectively.

Ionization channel	I	II	III	IV	V	VI
$Q_{6a}$	0	0	0	0	0.48	0.48
Singlet state	$S_2$ ( ${}^1B_{2u}$ )	$S_2$	$S_2$	$S_2$	$S_1$ ( ${}^1B_{3u}$ )	$S_1$
Doublet state	$D_6$ ( ${}^2B_{2u}$ )	$D_5$ ( ${}^2B_{3u}$ )	$D_3$ ( ${}^2B_{2g}$ )	$D_1$ ( ${}^2B_{1g}$ )	$D_4$ ( ${}^2B_{3u}$ )	$D_0$ ( ${}^2A_g$ )
$\epsilon_c$	0.05	0.25	2.52	3.95	0.33	4.00
Ionizing orbital	$6a_g$	$1b_{1g}$	$1a_u$	$2b_{3u}$	$6a_g$	$2b_{3u}$
VII	VIII	IX	X	XI		
0.77	0.77	0.77	1.59	1.59		
$S_3$ ( ${}^1A_u$ )	$S_3$	$S_3$	$S_4$ ( ${}^1B_{2g}$ )	$S_4$		
$D_6$	$D_7$ ( ${}^2B_{1u}$ )	$D_0$	$D_4$	$D_2$ ( ${}^2B_{1u}$ )		
0.18	0.23	4.90	1.63	3.92		
$1b_{2g}$	$1b_{1g}$	$1a_u$	$5b_{1u}$	$2b_{3u}$		

at the Franck-Condon position  $Q_{6a} = 0$  and those from  $S_1$ ,  $S_3$ , and  $S_4$  at their potential minima  $Q_{6a} = 0.48$ ,  $0.77$ , and  $1.59 u^{1/2}a_0$ , respectively. The resultant spectra are plotted in Fig. 2(b). Those from  $S_2$  and  $S_1$  are analogous to the experimental spectra for delay times 1 and 49 fs, respectively, except for relatively low intensity of the near-threshold component due to the plane-wave approximation for a photoelectron wave function. This agrees with the results of our nuclear wave packet simulations [24], which advocated the direct nonradiative transition pathway  $S_2 \rightarrow S_1$ , and also with the measured  $S_2$  lifetime of about 20 fs [5,6]. Though all energetically open ionization channels indicated in Fig. 1 were included in the summation of Eq. (4), those with a zero or rather small photoionization coupling matrix element are invisible in the calculated photoelectron spectra. Ionization channels that constitute the spectral peaks in Fig. 2(b) are summarized in Table 2.

We first analyze the spectrum from  $S_2$ . The first peak centered at 0.3 eV is composed of two ionization channels. One is  $D_6 \leftarrow S_2$  (Channel I), for which the difference between the corresponding potential energy curves in Fig. 1 (hereafter denoted as  $\epsilon_c$ ) is 0.05 eV. The existence of Channel I has been deduced in Ref. [25] from the Koopmans picture, in which photoionization involves a single active electron and leaves the electron configuration of the residual core unchanged. Table 3 presents dominant electron configurations of the singlet and doublet states

**Table 3**

Dominant electron configurations of the singlet and doublet states listed in Table 2. The absolute values of their CI coefficients at the Franck-Condon position  $Q_{6a} = 0$  are provided.

State	Dominant configuration(s)	CI coefficient (absolute value)
$D_7$ ( ${}^2B_{1u}$ )	$(6a_g)^{-1} (1b_{1g})^{-1} (1a_u)^{+1}$	0.70, 0.40 <sup>a</sup>
$D_6$ ( ${}^2B_{2u}$ )	$(6a_g)^{-1} (1b_{1g})^{-1} (2b_{3u})^{+1}$	0.66, 0.47 <sup>a</sup>
$D_5$ ( ${}^2B_{3u}$ )	$(1b_{3u})^{-1}$	0.71
	$(1b_{1g})^{-2} (2b_{3u})^{+1}$	0.36
$D_4$ ( ${}^2B_{3u}$ )	$(6a_g)^{-2} (2b_{3u})^{+1}$	0.75
	$(5b_{1u})^{-2} (2b_{3u})^{+1}$	0.43
$D_3$ ( ${}^2B_{2g}$ )	$(1b_{2g})^{-1}$	0.86
$D_2$ ( ${}^2B_{1u}$ )	$(5b_{1u})^{-1}$	0.82
$D_1$ ( ${}^2B_{1g}$ )	$(1b_{1g})^{-1}$	0.86
$D_0$ ( ${}^2A_g$ )	$(6a_g)^{-1}$	0.85
$S_4$ ( ${}^1B_{2g}$ )	$(5b_{1u})^{-1} (2b_{3u})^{+1}$	0.78
	$(1b_{2g})^{-1} (6a_g)^{-1} (2b_{3u})^{+2}$	0.35
$S_3$ ( ${}^1A_u$ )	$(6a_g)^{-1} (1a_u)^{+1}$	0.83
$S_2$ ( ${}^1B_{2u}$ )	$(1b_{1g})^{-1} (2b_{3u})^{+1}$	0.69
	$(1b_{2g})^{-1} (1a_u)^{+1}$	0.45
$S_1$ ( ${}^1B_{3u}$ )	$(6a_g)^{-1} (2b_{3u})^{+1}$	0.84

<sup>a</sup> Electron configurations involving three unpaired electrons give rise to two doublet configuration state functions.

participating in the ionization channels. According to Table 3, under an independent electron approximation, Channel I can be viewed mainly as the ionization of an electron occupying the  $6a_g$  orbital, *i.e.*, the  $(6a_g)^{-1}$  process. Our theoretical results corroborate the emergence of Channel I assumed by Horio et al. [25]. The other channel for the first peak is  $D_5$  ( ${}^2B_{3u}$ )  $\leftarrow$   $S_2$  (Channel II,  $\epsilon_c = 0.25$  eV), which can be regarded as  $(1b_{1g})^{-1}$ . Channel II was not anticipated in Ref. [25]. This suggests a possibility of the participation of Channel II. The second peak at 2.3 eV, which is a clear signature of  $S_2$ , originates from  $D_3$  ( ${}^2B_{2g}$ )  $\leftarrow$   $S_2$  [Channel III,  $\epsilon_c = 2.52$  eV,  $(1a_u)^{-1}$ ]. The third one at 4 eV is attributed to  $D_1 \leftarrow S_2$  [Channel IV,  $\epsilon_c = 3.95$  eV,  $(2b_{3u})^{-1}$ ]. The absence of the  $D_0 \leftarrow S_2$  process, which is forbidden in the crude Koopmans picture, is consistent with the fact that its contribution to the measured spectra is minor [25].

Next, in the spectrum from  $S_1$ , there are two peaks at 0.4 and 4 eV that energetically overlap with the first and third ones for  $S_2$ , respectively. The former stems from  $D_4$  ( ${}^2B_{3u}$ )  $\leftarrow$   $S_1$  [Channel V,  $\epsilon_c = 0.33$  eV,  $(6a_g)^{-1}$ ] and the latter is due to  $D_0 \leftarrow S_1$  [Channel VI,  $\epsilon_c = 4.00$  eV,  $(2b_{3u})^{-1}$ ]. Apart from the newly discovered Channel II, all these analyses of the  $S_2$  and  $S_1$  photoelectron spectra, which respectively correspond to the experimental ones for delay times 1 and 49 fs, basically agree with the peak assignments in Ref. [25]. Moreover, the calculated spectra for  $S_2$  and  $S_1$  qualitatively reproduce the observed enhancements of the first and third bands shown in Fig. 2(a) despite the above-mentioned underestimation of the near-threshold component. The blue (high-energy) shift of the first band is also described to some extent, while the red (low-energy) shift of the third one is not. The lowering of singlet excited-state energies by 0.53 eV properly corrected the difference in potential energy curves between  $D_1$  and  $S_2$  but still underestimated that between  $D_0$  and  $S_1$ . One can see this in Table 1; the corrected adiabatic ionization energy for  $D_0 \leftarrow S_1$  is 5.27 eV, which is less than the experimental value (5.46 eV). As a result,  $\epsilon_c$  for Channel VI is a little overestimated and thus the red shift of the third band is not reproduced in Fig. 2(b).

In marked distinction from the cases of  $S_2$  and  $S_1$ , the spectra from  $S_3$  and  $S_4$  exhibit peaks at totally different positions from the experimental ones. For  $S_3$ , the peak overlapping with the first one for  $S_2$  at 0.3 eV is constituted by  $D_6 \leftarrow S_3$  [Channel VII,  $\epsilon_c = 0.18$  eV,  $(1b_{2g})^{-1}$ ] and  $D_7$  ( ${}^2B_{1u}$ )  $\leftarrow$   $S_3$  [Channel VIII,  $\epsilon_c = 0.23$  eV,  $(1b_{1g})^{-1}$ ]. The former corresponds to  $(1b_{2g})^{-1}$  because  $D_6$  contains a minor contribution from the electron configuration denoted as  $(1b_{2g})^{-1} (6a_g)^{-1} (1a_u)^{+1}$ , whose CI coefficient has an absolute value of about 0.2. It is most striking that the strongest peak in the four calculated spectra is located at about 5 eV, which is ascribed to  $D_0 \leftarrow S_3$  [Channel IX,  $\epsilon_c = 4.90$  eV,  $(1a_u)^{-1}$ ]. If a rapid and substantial transition took place from  $S_2$  to  $S_3$  on a time scale of 20 fs as proposed by Werner et al. [16] and Sala et al. [18,19], a

prominent peak or band should have appeared in this region of the experimental spectrum for longer delay time. The spectrum from  $S_4$  shows a peak at 1.6 eV arising from  $D_4 \leftarrow S_4$  [Channel X,  $\varepsilon_c = 1.63$  eV,  $(5b_{1u})^{-1}$ ] besides the other peak at 4 eV due to  $D_2 (^2B_{1u}) \leftarrow S_4$  [Channel XI,  $\varepsilon_c = 3.92$  eV,  $(2b_{3u})^{-1}$ ]. The former peak is stronger than the second one for  $S_2$ ; however, the characteristic band observed at 1.5–2.5 eV in Fig. 2(a) attenuates (finally disappears) with increasing delay time.

The similarity and difference among the eleven ionization channels are discussed from the viewpoint of Dyson orbitals in Appendix A. The photoelectron spectra from  $S_1$ ,  $S_3$ , and  $S_4$  in Fig. 2(b) are similar to the respective spectra calculated at the Franck-Condon position  $Q_{6a} = 0$  because the CI coefficients of the electron configurations in Table 3 hardly vary among the four geometries  $Q_{6a} = 0, 0.48, 0.77,$  and  $1.59 \text{ u}^{1/2} a_0$ . This indicates that the insights obtained from the present simulations are independent of the choice of molecular geometries along  $Q_{6a}$  at which photoelectron spectra are evaluated. The results in this paper confirm our previous finding from nuclear wave packet simulations [24], *i.e.*, no participation of  $S_3$  or  $S_4$  in the nonradiative decay of  $S_2$ .

#### 4. Conclusion and perspectives

In order to elucidate the contributions from the optically dark  $\pi\pi^*$  states  $S_1 (^1B_{3u})$ ,  $S_3 (^1A_u)$ , and  $S_4 (^1B_{2g})$  to the nonradiative decay of the optically bright  $\pi\pi^*$  state  $S_2 (^1B_{2u})$  in photo-excited pyrazine, we have theoretically analyzed its time-resolved photoelectron spectrum measured in the recent UV-pump VUV-probe experiment by Horio et al. [25]. To the best of our knowledge, this is the first report on the simulation of the VUV (as high as 9.3 eV) photoelectron spectrum of pyrazine. We evaluated the photoelectron spectra for ionization from each of the four excited states  $S_1, S_2, S_3,$  and  $S_4$  using the MRCISD wave functions and potential energy curves of the neutral and cationic states along the totally symmetric mode  $Q_{6a}$ . The calculated spectra from  $S_2$  and  $S_1$  were in good accord with the spectra observed before and after the  $S_2$  decay, respectively, while those from  $S_3$  and  $S_4$  were totally different from the experimental ones. We identified the ionization channels constituting the peaks in the four calculated spectra and discovered  $D_5 (^2B_{3u}) \leftarrow S_2$  (Channel II), which was not considered in the experimental peak assignments. All these results support one of the

important findings from our nuclear wave packet simulations presented in Ref. [24]: Nonadiabatic transitions from  $S_2$  to  $S_3$  and  $S_4$  are so small that the conventional two-state ( $S_2 \rightarrow S_1$ ) picture is valid.

The theoretical results presented in this paper have been obtained from single-point calculations at four representative geometries along  $Q_{6a}$ , *i.e.*, at the Franck-Condon position and the potential minima of  $S_1, S_3$  and  $S_4$ . The next step toward complete understanding of ultrafast internal conversion dynamics in pyrazine is to compute *time-resolved* VUV photoelectron spectrum and photoelectron angular distribution, which realizes a conclusive comparison with the experiment by Horio et al. [25]. They extracted the anisotropy parameter from the observed angular distributions as a function of delay time and photoelectron kinetic energy [25]. This serves as a quantitative measure to be compared with calculated time-resolved angular distributions. Out of the 24 vibrational modes of pyrazine only the out-of-plane CH bending mode  $Q_{10a} (b_{1g})$  couples  $S_2$  and  $S_1$ , and we have revealed the predominance of  $Q_{6a}$  and  $Q_{10a}$  over the other 22 modes during the  $S_2 \rightarrow S_1$  nonadiabatic transition [24]. The results of our nuclear wave packet simulations within the  $Q_{6a}$ – $Q_{10a}$  subspace [24] can therefore be utilized to calculate time-resolved VUV photoelectron spectrum and photoelectron angular distribution. In Ref. [24], we have also suggested a hypothesis that the transient lifetime of the  $S_2 \rightarrow S_1$  nonadiabatic transition through a conical intersection may be 7 fs. It is much faster than the measured  $S_2$  lifetime of about 20 fs [5,6], which includes the time to reach the conical intersection. Detailed analysis of the temporal behavior of the short-lived band at 1.5–2.5 eV with reference to the calculated time-resolved photoelectron spectrum will help to verify the hypothesis. This simulation is underway and will be reported elsewhere.

#### Acknowledgements

M.K. thanks Dr. T. Horio and Prof. T. Suzuki for providing us with their experimental data. This work was supported in part by JSPS KAKENHI Grant Numbers JP26810002 and JP16H04091. F.R. and B.M. acknowledge support from the Fonds National de la Recherche Scientifique, Belgium (F.R.S.-FNRS) and from the F.R.S.-FNRS research Grants T.0132.16 and J.0012.18. Computational resources have been provided by the Consortium des Equipements de Calcul Intensif (CECI), funded by the F.R.S.-FNRS under Grant No. 2.5020.11.

#### Appendix A. Dyson orbital analysis of ionization channels

The Dyson orbitals for the eleven ionization channels that contribute to the calculated photoelectron spectra in Fig. 2(b) are depicted in Fig. 3. Since the Dyson orbitals are defined as the overlap between neutral and cationic electronic states [see Eq. (3)], they reflect the character of the ionizing molecular orbital discussed in Section 3.2 and do not vary significantly with the molecular geometries sampled in the computations.

Nevertheless, the norms of Dyson orbitals, which affect spectral intensity as seen in Eq. (4), are not necessarily similar for different ionization channels. For example, let us compare the Dyson orbital norms for Channels III and IX, which are both  $(1a_u)^{-1}$ . The former is 0.19, which is much smaller than the latter (0.59) as shown in Fig. 3. The value of  $\varepsilon_c$ , which determines a spectral peak position, is also quite different between Channels III and IX (see Table 2). These manifest the breakdown of an independent electron approximation and significant electron correlation in the ionization channels.

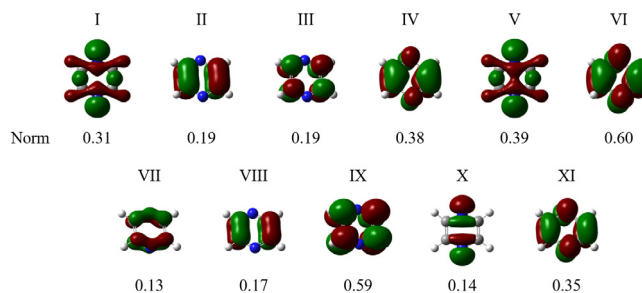


Fig. 3. Dyson orbitals for the eleven ionization channels summarized in Table 2. The white, gray, and blue balls represent hydrogen, carbon, and nitrogen atoms, respectively, of pyrazine.

## References

- [1] K.K. Innes, I.G. Ross, W.R. Moomaw, *J. Mol. Spectrosc.* 132 (1988) 492.
- [2] W. Domcke, D.R. Yarkony, H. Köppel (Eds.), *Conical Intersections*, World Scientific, Singapore, 2004.
- [3] T. Suzuki, Y. Suzuki, in: S. H. Lin, A. A. Villaeys, Y. Fujimura (Eds.), *Advances in Multi-Photon Processes and Spectroscopy*, World Scientific, Singapore, 2014, vol. 21, ch. 4, pp. 139–174.
- [4] I. Yamazaki, T. Murao, T. Yamanaka, K. Yoshihara, *Faraday Discuss. Chem. Soc.* 75 (1983) 395.
- [5] V. Stert, P. Farmanara, W. Radloff, *J. Chem. Phys.* 112 (2000) 4460.
- [6] Y. Suzuki, T. Fuji, T. Horio, T. Suzuki, *J. Chem. Phys.* 132 (2010) 174302.
- [7] R. Schneider, W. Domcke, *Chem. Phys. Lett.* 150 (1988) 235.
- [8] R. Schneider, W. Domcke, *Chem. Phys. Lett.* 159 (1989) 61.
- [9] G. Stock, R. Schneider, W. Domcke, *J. Chem. Phys.* 90 (1989) 7184.
- [10] R. Schneider, W. Domcke, H. Köppel, *J. Chem. Phys.* 92 (1990) 1045.
- [11] G. Stock, W. Domcke, *J. Chem. Phys.* 93 (1990) 5496.
- [12] M. Seel, W. Domcke, *J. Chem. Phys.* 95 (1991) 7806.
- [13] L. Seidner, G. Stock, A.L. Sobolewski, W. Domcke, *J. Chem. Phys.* 96 (1992) 5298.
- [14] C. Woywod, W. Domcke, A.L. Sobolewski, H.-J. Werner, *J. Chem. Phys.* 100 (1994) 1400.
- [15] G. Stock, C. Woywod, W. Domcke, T. Swinney, B.S. Hudson, *J. Chem. Phys.* 103 (1995) 6851.
- [16] U. Werner, R. Mitrić, T. Suzuki, V. Bonačić-Koutecký, *Chem. Phys.* 349 (2008) 319.
- [17] G. Tomasello, A. Humeniuk, R. Mitrić, *J. Phys. Chem. A* 118 (2014) 8437.
- [18] M. Sala, B. Lasorne, F. Gatti, S. Guérin, *Phys. Chem. Chem. Phys.* 16 (2014) 15957.
- [19] M. Sala, S. Guérin, F. Gatti, *Phys. Chem. Chem. Phys.* 17 (2015) 29518.
- [20] W.R. Wadt, W.A. Goddard III, *J. Am. Chem. Soc.* 97 (1975) 2034.
- [21] I.C. Walker, M.H. Palmer, *Chem. Phys.* 153 (1991) 169.
- [22] Y. Okuzawa, M. Fujii, M. Ito, *Chem. Phys. Lett.* 171 (1990) 341.
- [23] J.C. Tully, *J. Chem. Phys.* 93 (1990) 1061.
- [24] M. Kanno, Y. Ito, N. Shimakura, S. Koseki, H. Kono, Y. Fujimura, *Phys. Chem. Chem. Phys.* 17 (2015) 2012.
- [25] T. Horio, R. Spesyvtsev, K. Nagashima, R.A. Ingle, Y. Suzuki, T. Suzuki, *J. Chem. Phys.* 145 (2016) 044306.
- [26] V. Blanchet, M.Z. Zgierski, T. Seideman, A. Stolow, *Nature* 401 (1999) 52.
- [27] T. Horio, T. Fuji, Y. Suzuki, T. Suzuki, *J. Am. Chem. Soc.* 131 (2009) 10392.
- [28] S. Dilthey, S. Hahn, G. Stock, *J. Chem. Phys.* 112 (2000) 4910.
- [29] S. Hahn, G. Stock, *Phys. Chem. Chem. Phys.* 3 (2001) 2331.
- [30] Y. Suzuki, M. Stener, T. Seideman, *Phys. Rev. Lett.* 89 (2002) 233002.
- [31] Y. Suzuki, M. Stener, T. Seideman, *J. Chem. Phys.* 118 (2003) 4432.
- [32] U. Werner, R. Mitrić, V. Bonačić-Koutecký, *J. Chem. Phys.* 132 (2010) 174301.
- [33] B. Mignolet, R.D. Levine, F. Remacle, *Phys. Rev. A* 86 (2012) 053429.
- [34] T. Kuš, B. Mignolet, R.D. Levine, F. Remacle, *J. Phys. Chem. A* 117 (2013) 10513.
- [35] H.-J. Werner, P.J. Knowles, *J. Chem. Phys.* 82 (1985) 5053.
- [36] P.J. Knowles, H.-J. Werner, *Chem. Phys. Lett.* 115 (1985) 259.
- [37] H.-J. Werner, P.J. Knowles, *J. Chem. Phys.* 89 (1988) 5803.
- [38] P.J. Knowles, H.-J. Werner, *Chem. Phys. Lett.* 145 (1988) 514.
- [39] P.J. Knowles, H.-J. Werner, *Theor. Chim. Acta* 84 (1992) 95.
- [40] I.N. Levine, *Quantum Chemistry*, sixth ed., Prentice Hall, New Jersey, 2009, pp. 471–635.
- [41] H.-J. Werner, P.J. Knowles, G. Knizia, F.R. Manby, M. Schütz, P. Celani, T. Korona, R. Lindh, A. Mitrushenkov, G. Rauhut, K.R. Shamasundar, T.B. Adler, R.D. Amos, A. Bernhardsson, A. Berning, D.L. Cooper, M.J.O. Deegan, A.J. Dobbyn, F. Eckert, E. Goll, C. Hampel, A. Hesselmann, G. Hetzer, T. Hrenar, G. Jansen, C. Köppl, Y. Liu, A.W. Lloyd, R.A. Mata, A.J. May, S.J. McNicholas, W. Meyer, M.E. Mura, A. Nicklass, D.P. O'Neill, P. Palmieri, D. Peng, K. Pflüger, R. Pitzer, M. Reiher, T. Shiozaki, H. Stoll, A.J. Stone, R. Tarroni, T. Thorsteinsson, M. Wang, *MOLPRO, version 2012.1*, Cardiff, UK, 2012.
- [42] H.-J. Werner, P.J. Knowles, G. Knizia, F.R. Manby, M. Schütz, *WIREs Comput. Mol. Sci.* 2 (2012) 242.
- [43] C.M. Oana, A.I. Krylov, *J. Chem. Phys.* 131 (2009) 124114.
- [44] B.T. Pickup, *Chem. Phys.* 19 (1977) 193.
- [45] C.M. Oana, A.I. Krylov, *J. Chem. Phys.* 127 (2007) 234106.
- [46] G.M. Seabra, I.G. Kaplan, V.G. Zakrzewski, J.V. Ortiz, *J. Chem. Phys.* 121 (2004) 4143.
- [47] T.S. Kuhlman, W.J. Glover, T. Mori, K.B. Møller, T.J. Martínez, *Faraday Discuss.* 157 (2012) 193.
- [48] R. Bersohn, A.H. Zewail, *Ber. Bunsenges. Phys. Chem.* 92 (1988) 373.
- [49] F. Remacle, R.D. Levine, *Z. Phys. Chem.* 221 (2009) 647.
- [50] M. Oku, Y. Hou, X. Xing, B. Reed, H. Xu, C. Chang, C.-Y. Ng, K. Nishizawa, K. Ohshimo, T. Suzuki, *J. Phys. Chem. A* 112 (2008) 2293.
- [51] A. Bolovinos, P. Tsekeris, J. Philis, E. Pantos, G. Andritsopoulos, *J. Mol. Spectrosc.* 103 (1984) 240.